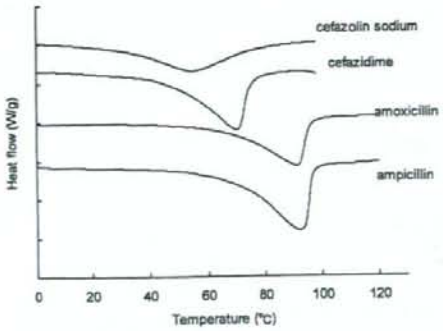

Figure 3. DSC thermograms for four antibiotic hydrates.

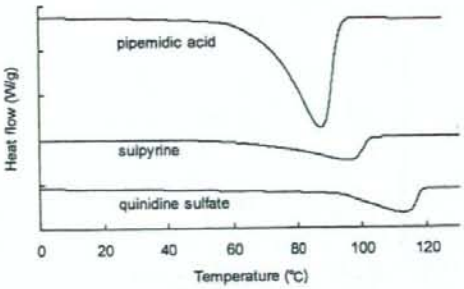

Figure 5. DSC thermograms for API hydrates showing a single endothermic peak.

Thus, determination of the molecular mobility of hydration water in API hydrates using NMR holds some challenges.

However, it is possible to determine the molecular mobility of hydration water in API hydrates by spin–spin relaxation measurement, if the spin–spin relaxation time (T_2) of the water protons is significantly different from that of the API protons. Furthermore, the spin–lattice relaxation time (T_1) of the water protons may be a useful indicator of water mobility, if the ratio of water protons to API protons is sufficiently large, or if the water protons have a correlation time (τ_c) corresponding to the T_1 minimum, such that the T_1 of the water proton is sensitively reflected in the measured T_1 value without being affected by spin diffusion between the water and the API protons. Moreover, even if the ratio of water protons to API protons is not particularly large, and even if water proton does not have a τ_c corresponding to the T_1 minimum, it may be possible to compare the molecular mobility of hydration water in API hydrates based on measured T_1 values, if both of the T_1 of the API proton and the ratio of water protons to API protons are similar for all of the API hydrates compared.

The purpose of this study was to examine the possibility of determining the molecular mobility of hydration water in API hydrates by NMR relaxation measurement. Spin–lattice relaxation, which reflects motions of MHz order, and spin–spin relaxation, which reflects slower motions, were measured for the 11 API hydrates listed in the Japanese Pharmacopeia (JP) using pulsed ^{1}H-NMR, which allows more simplified measurements than high-resolution ^{1}H-NMR. Furthermore, the ease of evaporation of the hydration water was determined under nonisothermal and isothermal conditions using DSC and water vapor sorption isotherm analysis, respectively, and the relationship between the ease of evaporation and the measured values of T_1 and T_2 was examined.

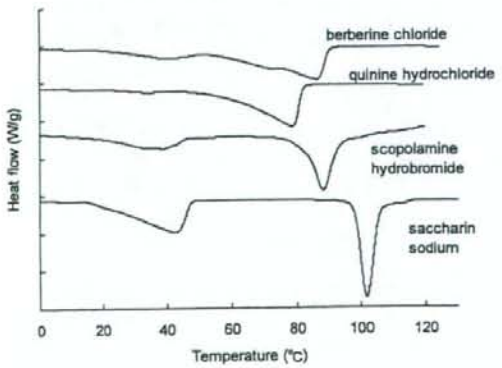

Figure 4. DSC thermograms for API hydrates showing two endothermic peaks.

EXPERIMENTAL

Materials

Cefazolin sodium, ceftazidime, amoxicillin, ampicillin, scopolamine hydrobromide, pipemidic acid, quinidine sulfate hydrates were purchased from Sigma Chemical Co. (St. Louis, MO), and berverine chloride, quinine hydrochloride, saccharin sodium, sulpyrine and di-sodium hydrogen phosphate 12 H_2O were purchased from Wako Pure Chemical Ind. Ltd. (Osaka, Japan), and di-sodium hydrogen phosphate 2 H_2O was from Merck (Darmstadt, Germany).

DOI 10.1002/jps

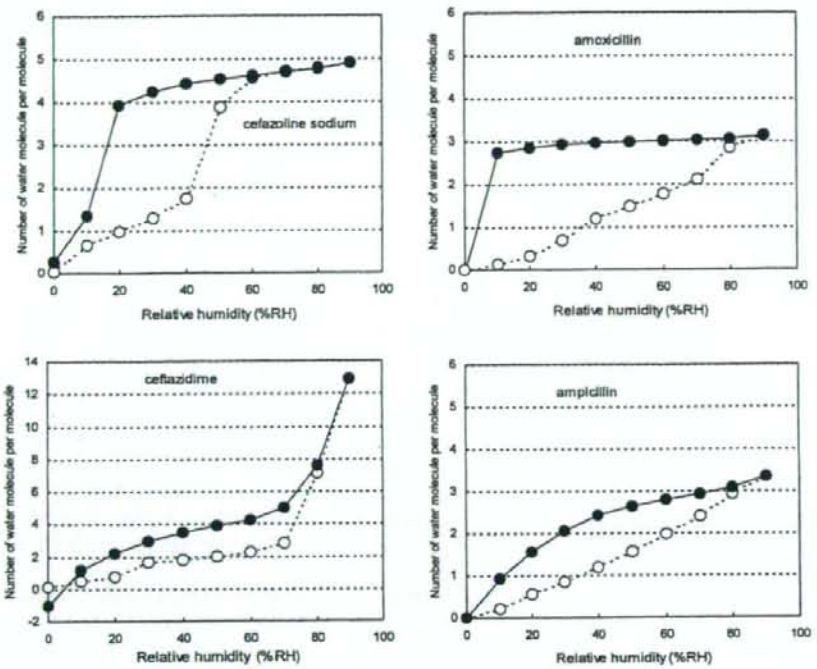

Figure 6. Water sorption isotherms for four antibiotic hydrates.

NMR Relaxation Times

The free induction decay (FID) of protons in API hydrates was obtained using a pulsed NMR spectrometer (25 MHz, JNM-MU25, JEOL, Tokyo, Japan). FID was obtained at 10, 20, 30, and 40°C. The 90° pulses were 2 μs in duration. The "solid echo," with an echo delay of 10 μs, was used in the detection stage of all measurements, in order to overcome the effects of the dead-time.[12] Measurement was repeated four times with a recycling time over five times of the T_1 value measured as described below.

The FID signals obtained between 2.6 and 100 μs that showed only Gaussian-type decay were fitted to Eq. (1) to calculate the T_2 of proton. FID signals obtained for quinidine sulfate and pipemidic acid hydrates showed a small diversion from Gaussian behavior (beat signal) in the final stage of relaxation, suggesting Abragam-type relaxation.[13] However, T_2 was calculated according to Eq. (1) for the purpose of comparison among API hydrates. The FID signals that show both Gaussian and Lorentzian decay patterns were fitted to Eq. (2) representing the summation of the Gaussian and Lorentzian equations.

$$I(t) = I_0 \exp\left[-\left(\frac{t}{T_2}\right)^2\right] \tag{1}$$

$$I(t) = I_0\left[P_G \exp\left(-\left(\frac{t}{T_{2(G)}}\right)^2\right) + P_L \exp\left(-\frac{t}{T_{2(L)}}\right)\right] \tag{2}$$

where $I(t)$ and I_0 are signal intensity at time t and time 0. $T_{2(G)}$ and $T_{2(L)}$ are T_2 for Gaussian decay and Lorentzian decay, respectively, and P_G and P_L are the proportion of protons that show Gaussian decay and Lorentzian decay, respectively.

The T_1 of proton in API hydrates was determined at 30°C by the inversion recovery method. T_1 was calculated according to Eq. (3).

$$I(t) = I_0\left(1 - 2\exp\left(-\frac{t}{T_1}\right)\right) \tag{3}$$

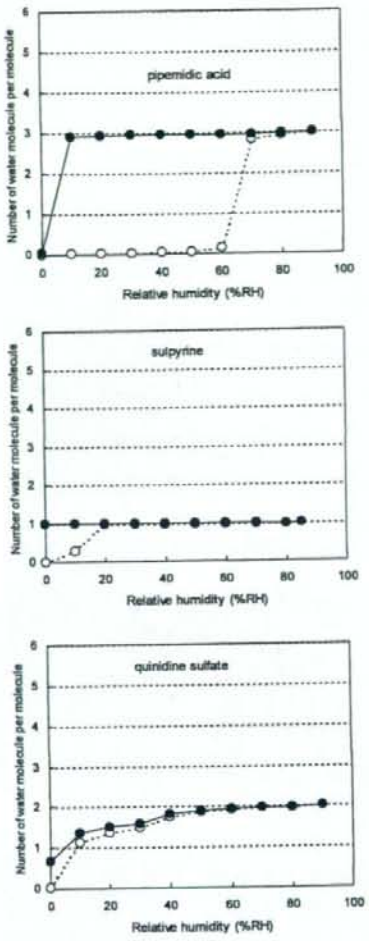

Figure 7. Water sorption isotherms for API hydrates showing a single endothermic peak in DSC thermogram.

Differential Scanning Calorimetry (DSC)

Modulated temperature DSC experiments were performed using a commercial system (2920; TA Instruments, New Castle, DE) attached to a refrigerated cooling accessory. The conditions were as follows: modulation period of 100 s, a modulation amplitude of ±0.5°C, and an underlying heating rate of 1°C/min. Temperature calibration was performed using indium. Samples (approximately 10 mg) were put in a pan without a lid. Nitrogen gas was flowed at 30 mL/min.

Water Sorption Isotherm

Water sorption isotherms were measured gravimetrically at 25°C using the automated sorption analyzer from VTI Corp. (Hialeah, FL). Prior to water sorption and desorption, samples were dried at 60°C and reduced pressure, until the partial vapor pressure became less than 0.0. Equilibrium water content was measured at ascending partial vapor pressures ranging from 0.10 to 0.95, then at descending partial vapor pressures ranging from 0.95 to 0.00 in steps of 0.10 or 0.05. Equilibrium was regarded to have been achieved once the change in sample weight was less than 0.001 mg over 10 min. The limit duration for measurement at a partial vapor pressure was 10 h for scopolamine hydrobromide and 5 h for the others.

RESULTS

NMR Relaxation Times

Figures 1 and 2 show representative examples of the time courses of spin–spin relaxation observed for the 11 API hydrates. Of the four antibiotic hydrates, all exhibited both Gaussian-type decay and Lorentzian decay, as exemplified by ceftazidime and cefazolin sodium hydrates (Fig. 1). The other seven API hydrates exhibited only Gaussian-type decay, as exemplified by quinidine sulfate and scopolamine hydrobromide hydrates (Fig. 2).

In order to calculate the proportion of water protons to API protons, which is required to obtain the T_2 of the water protons by curve-fitting of decay patterns, the number of water molecules per API hydrate molecule was measured by the Karl Fischer method. The results are shown in Table 1, in which the values specified in the JP are also noted for the purpose of comparison. The measured water contents were consistent with those specified in the JP for pipemidic acid, sulpyrine, and quinidine sulfate hydrates, as well as all antibiotic hydrates except for cefazolin sodium hydrate. In contrast, quinine hydrochloride, scopolamine hydrobromide, and saccharin sodium hydrates showed smaller water contents than those specified in the JP.

The time courses of spin–spin relaxation showing both Gaussian decay and Lorentzian decay observed for the four antibiotic hydrates were well fitted to Eq. (2) using the proportion of water protons calculated from the measured water

DOI 10.1002/jps

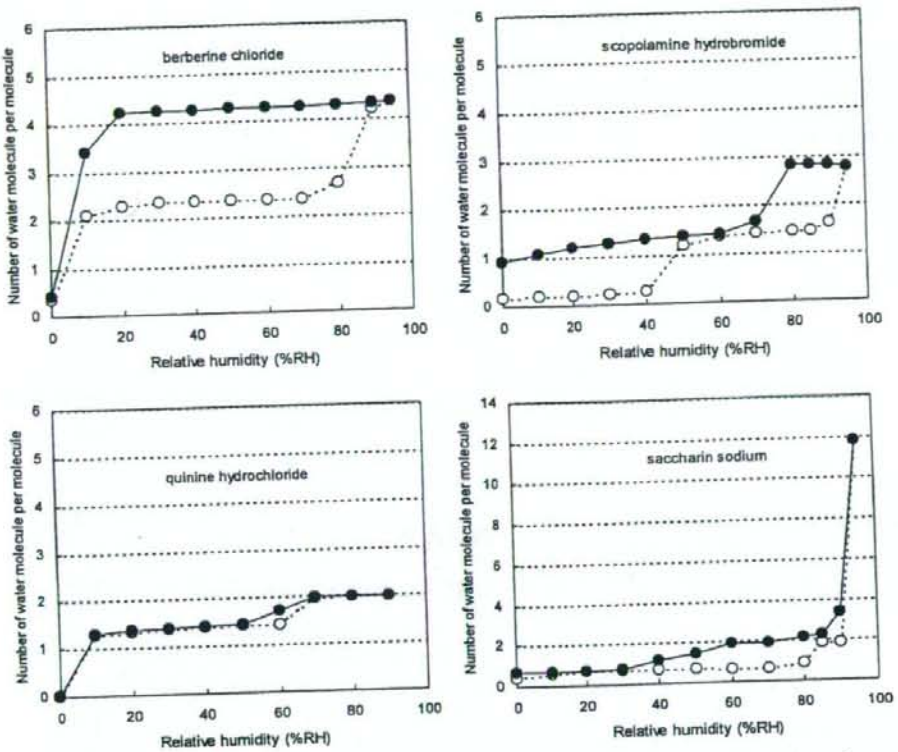

Figure 8. Water sorption isotherms for API hydrates showing two endothermic peaks in DSC thermogram.

content, as shown by the regression curve in Figure 1. Therefore, all of the water protons in the molecule are considered to show Lorentzian decay, and the Gaussian decay is attributed to the drug protons. The T_2 of the Lorentzian decay was calculated according to Eq. (2), and the results will be discussed below. For cefazolin sodium hydrate, better curve-fitting was obtained by regression analysis using a slightly larger value for the proportion of water protons than that calculated from the measured water content. This suggests that a small number of the drug protons exhibit Lorentzian decay; however, it is possible that the water content of the sample used for NMR measurement was different from that of the sample used for Karl Fischer measurements.

The seven API hydrates other than the antibiotic hydrates did not exhibit Lorentzian decay, indicating that all water protons and drug protons in the molecule showed Gaussian decay. The T_2 of the water protons was calculated according to Eq. (1), assuming that the T_2 of the drug protons is similar to that of the water protons. The results will be discussed below.

DSC Thermograms

Figures 3–5 show DSC thermograms measured for the 11 API hydrates. The four antibiotic hydrates, which exhibited Lorentzian decay upon spin–spin relaxation, showed a single endothermic peak due to water evaporation, as shown in Figure 3. In contrast, the API hydrates that did not exhibit Lorentzian decay showed two endothermic peaks (Fig. 4), or one peak (Fig. 5).

The temperature at which an endothermic peak due to water evaporation is observed may be considered to represent the ease of evaporation of hydration water under nonisothermal conditions. The onset temperature was determined as a parameter for approximate comparison of ease of evaporation among the API hydrates, along with ease of evaporation under isothermal conditions as

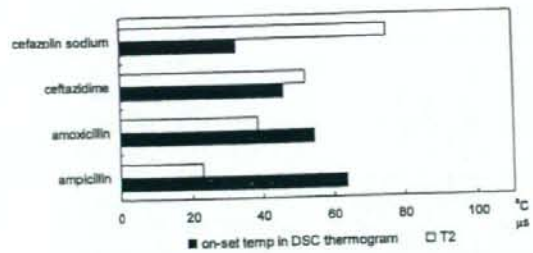

Figure 9. Correlation between onset temperature and T_2 for four antibiotic hydrates.

determined by water vapor sorption analysis. Onset temperature is known to depend on various factors, such as the heating rate, the shapes of the pan and lid, the surface area of the sample, and the flow rate of nitrogen gas. In this study, controllable factors such as the heating rate and the flow rate of nitrogen gas were kept constant, and a pan without a lid was used. The onset temperatures obtained will be discussed below.

Water Vapor Sorption Isotherm

Figures 6–8 show water sorption isotherms observed for the four antibiotic hydrates, the other three API hydrates that exhibited a single endothermic peak due to water evaporation, and the four API hydrates that exhibited two peaks due to water evaporation, respectively. The y-axis represents the number of water molecules per API hydrate molecule, calculated from the water content measured by the Karl Fischer method, assuming that all water molecules present in the sample were evaporated during the drying process (60°C, reduced pressure) prior to the sorption and desorption processes.

The water sorption isotherms (Fig. 6) observed for the four antibiotic hydrates, which exhibited Lorentzian decay upon spin–spin relaxation, indicate that during the desorption process, the water content decreased with decreasing humidity in the range 90–0% RH, with a significant slope in the water content versus humidity plot.

Among the three API hydrates that did not exhibit Lorentzian decay and showed a single endothermic peak due to water evaporation, pipemidic acid and sulpyrine hydrates gave water desorption isotherms in which the water content was constant over a wide humidity range, as shown in Figure 7. Quinidine sulfate also showed a flat line in the water content versus humidity plot, though it was observed only at high humidities.

The water desorption isotherms observed for the other four API hydrates (except berberine chloride), which did not exhibit Lorentzian decay and showed two endothermic peaks due to water evaporation, indicated that the water content remained approximately constant at two levels (Fig. 8).

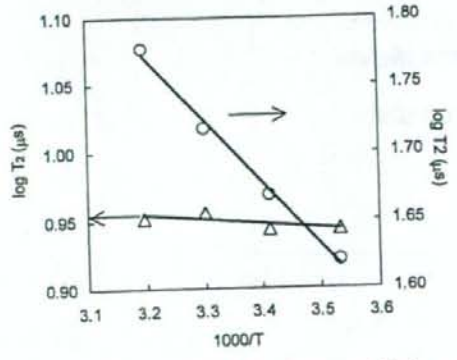

Figure 10. Temperature dependence of T_2 for ceftazidime (circle) and pipemidic acid (triangle) hydrates.

DISCUSSION

The molecular mobility of hydration water in API hydrates was found to vary over a wide range; some, such as ceftazidime hydrate, contain hydration water that shows Lorentzian decay upon spin–spin relaxation, while others contain hydration water that shows Gaussian decay.

Hydration Water Showing Lorentzian Decay

All of the water molecules present in the four antibiotic hydrates were found to exhibit Lorentzian decay, because the proportion of Lorentzian decay was consistent with the proportion of water protons calculated from the water content measured by the Karl Fischer method (Fig. 1). The finding that the water molecules in the antibiotic hydrates showed Lorentzian decay rather than Gaussian decay suggests that water molecules are held in voids in the crystal, rather than being firmly trapped in the crystal lattice. These water molecules may evaporate through channels formed in the interior of the crystal.[14] Hydration water that requires more energy to be released

DOI 10.1002/jps

may exhibit a higher onset temperature of the endothermic peak due to water evaporation in DSC.

The T_2 values determined based on Lorentzian decay is related with τ_c by Eq. (4), such that a smaller value of T_2 represents a larger τ_c (lower mobility).

$$\frac{1}{T_2} = \frac{\gamma^4 \hbar^2 I(I+1)}{5r^6}\left(3\tau_c + \frac{5\tau_c}{1+\omega_0^2\tau_c^2} + \frac{2\tau_c}{1+4\omega_0^2\tau_c^2}\right) \quad (4)$$

where γ, ω_0, I, r, and $\hbar$ are the gyromagnetic ratio, resonance frequency, spin quantum number, spin distance, and the Plank's constant divided by 2π.

As shown in Figure 9, T_2 increased as the onset temperature (Fig. 3) decreased, indicating that hydration water which evaporates at lower temperatures has greater molecular mobility as determined by T_2. This correlation between T_2 and the ease of evaporation under nonisothermal conditions may be explained by assuming that hydration water with a greater T_2 (higher mobility) can escape through channels at a lower temperature.

In order to gain further insight into the correlation between ease of evaporation and the molecular mobility of the hydration water, the ease of evaporation under isothermal conditions was evaluated by water sorption isotherm measurement. Each of the four antibiotic hydrates exhibited a desorption isotherm showing decreases in water content associated with decreases in humidity (Fig. 6). As discussed below, the crystal form of ampicillin hydrate appeared to be altered during the drying process prior to the measurement of water sorption isotherms. Therefore, the isotherm obtained for ampicillin could not be compared with the NMR and DSC data. However, such detrimental effect of predrying was not observed for the other three antibiotic hydrates. The negative water content observed after the desorption process for ceftazidime may be due to chemical degradation occurred under high-humidity conditions or incomplete evaporation of hydration water during predrying. Compared to amoxicillin hydrate, cefazolin sodium hydrate, which has a larger T_2 value, exhibited a greater slope in its water content versus humidity plot. Furthermore, cefazolin sodium exhibited rapid dehydration when humidity was decreased below 20% RH, whereas amoxicillin did not exhibit rapid dehydration until humidity was decreased below 10% RH. These findings suggest that the ease of evaporation of hydration water under isothermal conditions is correlated with molecular mobility as determined by T_2, which supports the conclusion obtained based on DSC measurement. For ampicillin, the slope of the water content versus humidity plot was greater than that of amoxicillin hydrate despite its lower molecular mobility as determined by T_2 and higher onset temperature. This suggests that the drying conditions prior to the sorption and desorption processes were inadequate, which may result in destruction of the crystalline structure. Thus, the isotherm obtained for ampicillin could not be compared with the NMR and DSC data.

As exemplified by ceftazidime hydrate (Fig. 10), T_2 increased significantly with increasing temperature, indicating that T_2 reflects the increases in molecular mobility associated with increases in temperature. Thus, molecular mobility can be considered to correlate with T_2. As shown in Figure 11, antibiotic hydrates with smaller T_2

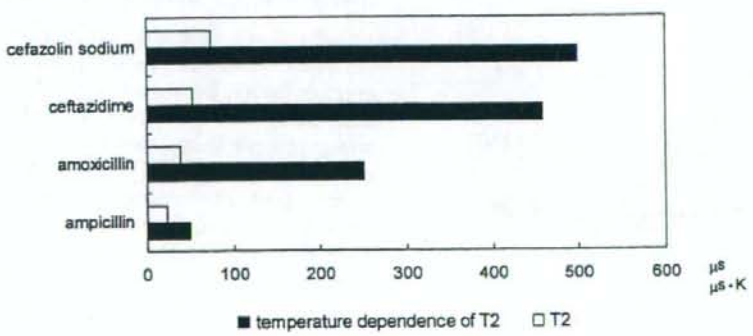

Figure 11. Correlation between T_2 and temperature dependence of T_2 for four antibiotic hydrates.

values showed a smaller change in T_2 with temperature change. This finding suggests that lower values of T_2 reflect a smaller scale of molecular motion, with lower activation energies.

Spin–lattice relaxation time (T_1) is known to reflect molecular mobility, similarly to T_2, but increases with decreasing T_2 (with decreasing molecular mobility) in the slow motional regime. The T_1 values of water protons in the presence of drug protons cannot be determined due to spin diffusion, but an approximate determination of T_1 for water protons is possible if the proportion of water protons is large. For example, in $Na_2HPO_4 \cdot 12H_2O$ and $Na_2HPO_4 \cdot 2H_2O$, water protons are predominant (24/25 and 4/5, respectively). $Na_2HPO_4 \cdot 12H_2O$ exhibits slower spin–spin relaxation (larger T_2) (Fig. 12), and faster spin–lattice relaxation (smaller T_1) (Fig. 13) compared to $Na_2HPO_4 \cdot 2H_2O$, which indicates that both T_1 and T_2 reflect the molecular mobility of hydration water. For the antibiotic hydrates examined, however, correlations between T_1 and T_2 were not observed, as shown in Figure 14. This finding indicates that for API hydrates containing a significant amount of drug protons, such as antibiotic hydrates, the molecular mobility of the hydration water is not reflected in T_1.

Hydration Water Showing Gaussian Decay

As mentioned previously, all of the API hydrates other than the four antibiotic hydrates exhibited only Gaussian decay (Fig. 2). The value of T_2 did not vary significantly among the API hydrates, as shown in Figure 15. Furthermore, the onset temperatures of the single endothermic peaks

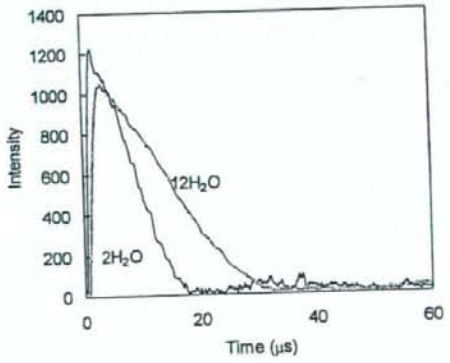

Figure 12. Free induction decay for Na_2HPO_4 $12H_2O$ and $2H_2O$.

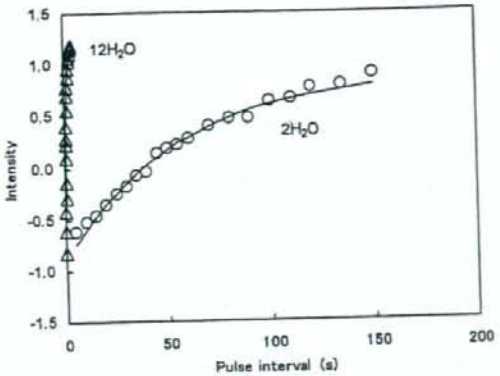

Figure 13. Spin–lattice relaxation for Na_2HPO_4 $12H_2O$ and $2H_2O$.

due to water evaporation for quinidine sulfate, pipemidic acid, and sulpyrine hydrates (Fig. 5), as well as each of the two peaks due to water evaporation observed for quinine hydrochloride, scopolamine hydrobromide, saccharin sodium, and berberine chloride hydrates (Fig. 4), were not correlated with T_2. These findings indicate that the molecular mobility of hydration water that shows Gaussian decay is too low to be reflected in T_2. No correlation between T_2 and molecular mobility is supported by the finding that changes in T_2 associated with changes in temperature were much smaller than those observed for the antibiotic hydrates that exhibited Lorentzian decay, as exemplified by pipemidic acid (Fig. 10). Such low molecular mobility may be attributed to water molecules firmly trapped in the crystal lattice, rather than water molecules trapped in voids in the crystal.

For quinidine sulfate, pipemidic acid, and sulpyrine hydrates, a single endothermic peak was observed in DSC (Fig. 5). The water content versus humidity plots showed a flat line at a certain number of water molecules. Pipemidic acid and sulpyrine showed a flat line at three and one water molecule(s) per hydrate, respectively, and evaporation of these water molecules was observed only under very low humidity (Fig. 7). These findings indicate that water molecules are firmly trapped in the crystal.

For quinine hydrochloride, scopolamine hydrobromide, saccharin sodium, and berberine chloride hydrates, two endothermic peaks were shown in DSC (Fig. 4). The water content versus humidity plots for these hydrates (except for berberine chloride) showed flat lines at two levels

DOI 10.1002/jps

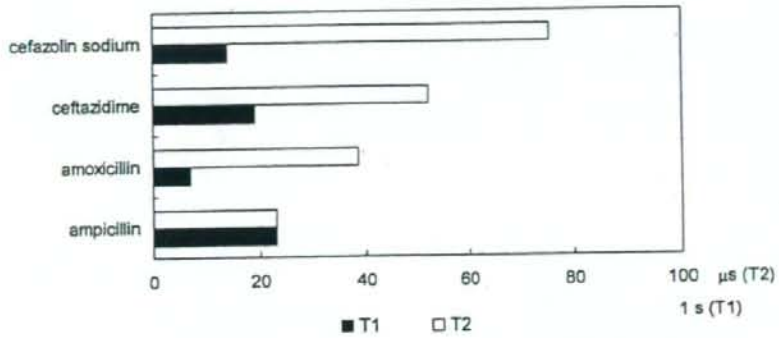

Figure 14. Correlation between T_1 and T_2 for four antibiotic hydrates.

of water content (Fig. 8), suggesting the presence of two water populations: molecules that evaporate at high humidity, and others that evaporate at lower humidity (below 10% RH). This seems to be consistent with the observation of two endothermic peaks in DSC. The endothermic peak observed at a high temperature and the flat line observed at a low humidity may be attributable to hydration water with strong hydrogen–bonding interactions, while the one observed at a lower temperature and higher humidity may be attributable to hydration water with week interactions. The presence of hydration water with week interactions is also supported by the finding that the water contents as measured by the Karl Fischer method were smaller than those specified in the JP (Tab. 1).

CONCLUSION

It was found that spin–spin relaxation time, T_2, is a useful parameter that can indicate the molecular mobility of water of hydration which has relatively high mobility and shows Lorentzian decay upon spin–spin relaxation. For these water molecules, molecular mobility as determined by T_2 is correlated with ease of evaporation both under nonisothermal and isothermal conditions,

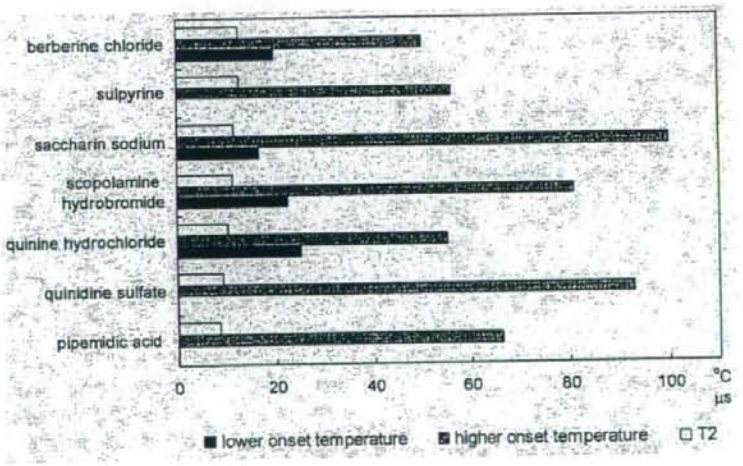

Figure 15. Correlation between onset temperature and T_2 for API hydrates that show Gaussian decay.

such that water molecules with greater ease of evaporation have higher T_2 values.

In contrast, for hydration water that has low mobility and shows Gaussian decay, T_2 was found not to correlate with ease of evaporation under nonisothermal conditions, suggesting that molecular motion that determines the ease of evaporation is not reflected in T_2; in this case, T_2 cannot be used as a parameter to indicate molecular mobility.

The water molecules in the API hydrates studied were found to have wide-ranging molecular mobilities, from low molecular mobility that could not be evaluated by NMR relaxation times, such as the water molecules in pipemidic acid hydrate, to high molecular mobility that could be evaluated by NMR relaxation times, such as the water molecules in ceftazidime hydrate.

REFERENCES

1. Yoshioka S, Aso Y. 2007. Correlations between molecular mobility and chemical stability during storage of amorphous pharmaceuticals. J Pharm Sci 96:960–981.
2. Ahlneck C, Zografi G. 1990. The molecular basis for moisture effects on the physical and chemical stabiity of drugs in the solid state. Int J Pharm 62:87–95.
3. Mimura H, Gato K, Kitamura S, Kitagawa T, Kohda S. 2002. Effect of water content on the solid-state stability in two isomorphic clathrates of cephalosporin: Cefazolin sodium pentahydrte (α form) and KF041 hydrate. Chem Pharm Bull 50: 766–770.
4. Zografi G. 1988. States of water associated with solids. Drug Dev Ind Pharm 14:1905–1926.
5. Newman AW, Reutzel-Edens SM, Zografi G. 2007. Characterization of the "hygroscopic" properties of active pharmaceutical ingredients. J Pharm Sci DOI: 10.1002/jps.21033.
6. Brittain HG, Grant DJW. 1999. Effect of polymorphism and solid state solvation on solubility and dissolution rate. In: Brittain HG, editor. Polymorphism in pharmaceutical solids. New York: Marcel Dekker. pp 279–330.
7. Shinyashiki N, Asaka N, Mashimo S. 1990. Dielectric study on dynamics of water in polymer matrix using a frequency range 10^6–10^{10} Hz. J Chem Phys 93:760–764.
8. Ahlqvist MU, Taylor LS. 2002. Water dynamics in channel hydrates investigated using H/D exchange. Int J Pharm 241:253–261.
9. Ruan R, Chen PL. 1998. Mobility of water in food and biological systems. In: Water in foods and biological materials, a nuclear magnetic resonance approach. Lancaster, PA: Technomic Publishing Company, Inc. pp 149–228.
10. Oksanen CA, Zografi G. 1993. Molecular mobility in mixtures of absorbed water and solid poly(vinylpyrrolidone). Pharm Res 10:791–799.
11. Otsuka T, Yoshioka S, Aso Y, Kojima S. 1995. Water mobility in aqueous solutions of macromolecular pharmaceutical excipients measured by oxygen-17 nuclear magnetic resonance. Chem Pharm Bull 43:1221–1223.
12. Mansfield P. 1965. Multiple-pulse nuclear magnetic resonance transients in solids. Phys Rev 137:A961–A974.
13. Parizel N, Meyer G, Weill G. 1993. Nuclear magnetic resonance linesahape studies of interpenetrating polymer networks. Polymer 12:2495–2502.
14. Morris KR. 1999. Structural aspects of hydrates and solvates. In: Brittain HG, editor. Polymorphism in pharmaceutical solids. New York: Marcel Dekker. pp 125–181.

DOI 10.1002/jps

Available online at www.sciencedirect.com
ScienceDirect
International Journal of Pharmaceutics 336 (2007) 191–195
INTERNATIONAL JOURNAL OF PHARMACEUTICS
www.elsevier.com/locate/ijpharm

Note

Crystallization rate of amorphous nifedipine analogues unrelated to the glass transition temperature

Tamaki Miyazaki *, Sumie Yoshioka, Yukio Aso, Toru Kawanishi

National Institute of Health Sciences, 1-18-1 Kamiyoga, Setagaya-ku, Tokyo 158-0851, Japan

Received 14 August 2006; received in revised form 12 October 2006; accepted 18 November 2006
Available online 28 November 2006

Abstract

To examine the relative contributions of molecular mobility and thermodynamic factor, the relationship between glass transition temperature (T_g) and the crystallization rate was examined using amorphous dihydropyridines (nifedipine (NFD), *m*-nifedipine (*m*-NFD), nitrendipine (NTR) and nilvadipine (NLV)) with differing T_g values. The time required for 10% crystallization, t_{90}, was calculated from the time course of decreases in the heat capacity change at T_g. The t_{90} of NLV and NTR decreased with decreases in T_g associated with water sorption. The t_{90} versus T_g/T plots almost overlapped for samples of differing water contents, indicating that the crystallization rate is determined by molecular mobility as indicated by T_g. In contrast, differences in the crystallization rate between these four drugs cannot be explained only by molecular mobility, since the t_{90} values at a given T_g/T were in the order: NLV > NTR > NFD ≈ *m*-NFD. A lower rate was obtained for amorphous drugs with lower structural symmetry and more bulky functional groups, suggesting that these factors are also important. Furthermore, the crystallization rate of NTR in solid dispersions with poly(vinylpyrrolidone) (PVP) and hydroxypropyl methylcellulose (HPMC) decreased to a greater extent than expected from the increased T_g. This also suggests that factors other than molecular mobility affect the crystallization rate.

Keywords: Crystallization; Amorphous state; Nifedipine; Glass transition; Molecular mobility; Excipients

Preparation of poorly water-soluble pharmaceuticals into amorphous forms improves their solubility. However, amorphous solids are physically unstable because of their high energy state, and crystallization during storage presents a problem. The process of crystallization is known to comprise two major steps: nucleation and crystal growth, and the rates are generally governed by molecular mobility affecting the diffusion rate of molecules and thermodynamic factors such as the Gibbs free energy and nucleus/amorphous interfacial energy (Salcki-Gerhardt and Zografi, 1994; Hancock and Zografi, 1997; Rodríguez-Hornedo and Murphy, 1999; Andronis and Zografi, 2000; Ngai et al., 2000). Our previous studies demonstrated that the overall crystallization rate of nifedipine (NFD) for both the amorphous pure drug and solid dispersions with poly(vinylpyrrolidone) (PVP) had similar temperature dependence as the mean relaxation time calculated using the Adam-Gibbs-Vogel equation, suggesting that the molecular mobility of amorphous pharmaceuticals was one of the important factors affecting the crystallization rate (Aso et al., 2001, 2004). However, the crystallization rate of amorphous pharmaceuticals cannot be determined only by molecular mobility, as it has been reported that the susceptibility to crystallization of pharmaceuticals possessing quite different thermodynamic properties does not follow the order of the decrease in the glass transition temperature (T_g) (Zhou et al., 2002).

The purpose of the present study is to discuss the relative contributions of the molecular mobility and thermodynamic factors to the crystallization rates of dihydropyridines with different substituents, including NFD, *m*-nifedipine (*m*-NFD), nitrendipine (NTR) and nilvadipine (NLV) (Fig. 1). The overall crystallization rates of these drugs in the pure amorphous solids were measured under various relative humidity (RH) conditions to elucidate the effects of the substituents and water content on the crystallization rate. The crystallization rate of NTR was also determined in solid dispersions containing polymers (PVP and hydroxypropyl methylcellulose (HPMC)). Although some

* Corresponding author. Tel.: +81 3 3700 1141; fax: +81 3 3707 6950.
E-mail addresses: miyazaki@nihs.go.jp (T. Miyazaki), yoshioka@nihs.go.jp (S. Yoshioka), aso@nihs.go.jp (Y. Aso), kawanish@nihs.go.jp (T. Kawanishi).

0378-5173/$ – see front matter © 2006 Elsevier B.V. All rights reserved.
doi:10.1016/j.ijpharm.2006.11.052

	abbreviation	R_1	R_2	R_3	R_4
nifedipine	[NFD]	CH_3	CH_3	NO_2	H
m-nifedipine	[m-NFD]	CH_3	CH_3	H	NO_2
nitrendipine	[NTR]	CH_3	C_2H_5	H	NO_2
nilvadipine	[NLV]	CN	$(CH_3)_2CH$	H	NO_2

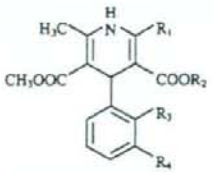

Fig. 1. Chemical structures of dihydropyridines.

papers have dealt with the crystallization of NTR and NLV in solid dispersions (Hirasawa et al., 2003a,b, 2004; Wang et al., 2005, 2006), few data are available that allow quantitative discussion about the relationship between molecular mobility and crystallization rates.

NFD and HPMC (USP grade) were purchased from Sigma Chemical Co. NTR, *m*-NFD and PVP (weight average molecular weight of 40000) were obtained from Wako Pure Chemical Industries Ltd. NLV was kindly supplied by Astellas Pharma Inc. The amorphous NFD, *m*-NFD, NTR, NLV and NTR solid dispersions with PVP and HPMC were prepared by melt quenching in the cell of a differential scanning calorimeter (DSC2920, TA Instruments). The crystalline drug or mixture of NTR and polymer (5 mg) was melted at a temperature approximately 20 °C above its melting point and then cooled to approximately 100 °C below the T_g at a cooling rate of 40 °C/min. Thermal and photo degradation of the drugs was checked by HPLC, and no change in the chromatograms was observed after the preparation in comparison with that before. Fig. 2 shows typical DSC thermograms for the four amorphous drugs immediately after preparation and after subsequent storage. The T_g values for the amorphous drugs were: NLV, 48.6 ± 0.3 °C; NFD, 46.2 ± 0.2 °C; *m*-NFD, 41.3 ± 0.1 °C; NTR, 32.4 ± 0.3 °C. As shown in Fig. 2(b), freshly prepared amorphous NFD exhibited two endothermic peaks at around 161 °C and 168 °C. The two melting points of the peaks agreed well with that for the metastable form II and stable form I, respectively (Burger and Koller, 1996). As shown in Fig. 2(c), the NFD sample, retaining an amorphous portion after 5 h storage at 60 °C, showed exothermic peaks due to crystallization of the amorphous phase and its transformation into a stable crystal, and melted at 168 °C, which is approximately the same temperature as the melting point of the intact crystal. As shown in Fig. 2(d), the sample stored at 60 °C for 46 h showed the exothermic peak around 120–140 °C due to transformation into a stable crystal, although change in the heat capacity (ΔC_p) at T_g was not significant. The exothermic peak around 120–140 °C due to transformation into a stable crystal was also observed during storage at 50 °C and 70 °C (thermogram not shown). These DSC thermograms suggested that amorphous NFD initially crystallized into a metastable form. Crystallization into the metastable form was also observed during storage at 50 °C and 70 °C (thermogram not shown). Amorphous *m*-NFD showed an exothermic peak due to crystallization but no obvious peak due to transformation into a stable form like that shown by the NFD samples, and melted at 206 °C, which is approximately the same temperature as the melting point of intact *m*-NFD (Fig. 2(f) and (g)). It is not clear from the DSC thermograms whether transition to a stable or a metastable crystalline form occurred during storage. Fig. 2(j) and (k) show the DSC thermograms of the partially crystallized NTR samples showing one melting peak at 128 °C. The observed melting point was lower than that of the stable crystal

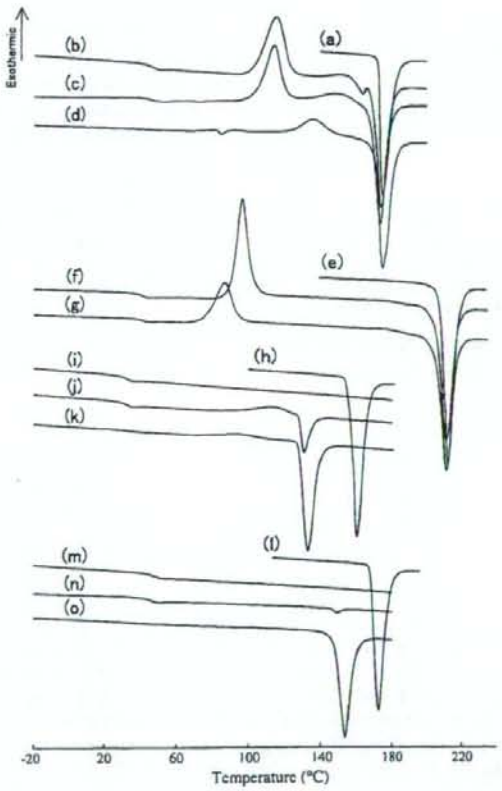

Fig. 2. Typical DSC thermograms: (a) NFD crystalline in the stable form, (b) freshly prepared amorphous NFD, (c) amorphous NFD after 5h-storage at 60 °C (d) amorphous NFD after 46 h-storage at 60 °C, (e) m-NFD crystalline in the stable form, (f) freshly prepared amorphous m-NFD, (g) amorphous m-NFD after 15 h-storage at 50 °C, (h) NTR crystalline in the stable form, (i) freshly prepared amorphous NTR, (j) amorphous NTR after 2 h-storage at 60 °C, (k) amorphous NTR after 9.75 h-storage at 60 °C, (l) NLV crystalline in the stable form, (m) freshly prepared amorphous NLV, (n) amorphous NLV after 48 h-storage at 80 °C, (o) amorphous NLV after 168 h-storage at 80 °C. Heating rate: 20 °C/min.

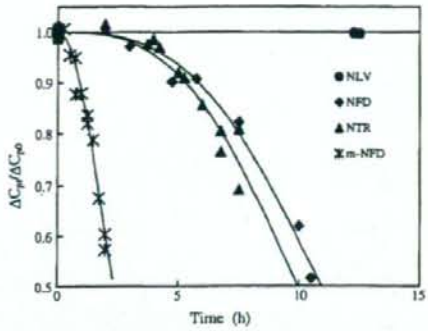

Fig. 3. Time profiles of crystallization for four dihydropyridines at 60 °C and 0%RH. The ratio of the amorphous form remaining at time t was calculated from the ΔC_p value assuming that the amount of amorphous phase is proportional to the ΔC_p. ΔC_{p0} and ΔC_{pt} are changes in ΔC_p at time 0 and t, respectively. Solid lines denote the fitting to the Avrami equation ($x(t) = \exp[-kt^n]$, $n = 3$).

(158 °C) and consistent with that reported for a metastable crystal (Kuhnert-Brandstätter and Völlenklee, 1986; Burger et al., 1997). As shown in Fig. 2(n) and (o), the partially crystallized NLV samples showed one melting peak at 148 °C. The observed melting point was lower than that for a stable crystal (168 °C) and similar to that for the dehydrated form of the monohydrate (Hirayama et al., 2000). Both amorphous NTR and NLV samples were considered to crystallize to their metastable crystalline forms under the conditions studied.

Fig. 3 shows the time profiles of crystallization of NFD, *m*-NFD, NTR, NLV at 60 °C and 0%RH. The crystallization rate was in the order: NLV < NTR = NFD < *m*-NFD. Fig. 4 shows the temperature dependence of the time required for 10% crystallization (t_{90}). Although NFD and NLV have approximately the same T_g, their values of t_{90} at the same temperature differed by more than two orders of magnitude (Fig. 4(A)). As shown in Fig. 4(B), the value of t_{90} at a given T_g/T (T being storage temperature) was in the order: NLV > NTR > NFD ≈ *m*-NFD within the whole range of temperature studied. As shown in Fig. 1, the four dihydropyridines have various alkyl groups at one of the carbonylester positions (R_2), and differ in the substitution position of the nitro group in the phenyl moiety (R_3 or R_4). The

Table 1
T_g values of amorphous NLV and NTR

RH (%)	T_g (°C)	
	NLV	NTR
0 (P_2O_5)	48.6 ± 0.3	32.4 ± 0.3
12 ($LiCl{\cdot}2H_2O$)	48.1 ± 0.7	30.5 ± 0.4
25 (CH_3COOK)	46.4 ± 0.5	29.0 ± 0.3
43 ($K_2CO_3{\cdot}2H_2O$)	43.4 ± 0.4	25.8 ± 0.3

For water absorption, the samples were kept at 5 °C for approximately 50 h in a desiccator containing saturated salt solutions. No crystallization was observed during the water absorption, as indicated by no endothermic melting peak in DSC thermograms.

bulkiness of R_2 shows the order: NFD, *m*-NFD (methyl) < NTR (ethyl) < NLV (isopropyl). Furthermore, the substituent at R_1 is a cyano group in NLV, whereas it is a methyl group in the other three drugs; thus, the structural symmetry of NLV is lower. Since the plots for NFD and *m*-NFD in Fig. 4(B) almost overlapped each other, the difference in the crystallization rate may be attributed to the difference in molecular mobility. In contrast, differences in the crystallization rate between NLV, NTR and NFD cannot be explained only by the difference in molecular mobility. The differences in structural symmetry and bulkiness of functional group may cause differences in the Gibbs free energy and nucleus/amorphous interfacial energy, resulting in the differing crystallization rates between these drugs.

The crystallization rate of amorphous NLV and NTR solids with differing T_g values due to differing water content was measured to elucidate the effect of T_g on the crystallization rate (Table 1). The partially crystallized NLV and NTR in the presence of water showed an endothermic melting peak at approximately 150 °C and 130 °C, respectively. This suggests that amorphous NLV and NTR containing water also crystallize into their metastable forms in a similar manner as shown for dry samples. Fig. 5(A) shows the temperature dependence of the t_{90} obtained for NLV and NTR in the presence of water. When compared at the same temperature, the t_{90} value decreased with increasing RH. As shown in Fig. 5(B), the t_{90} versus T_g/T plots for each drug overlapped with those obtained under dry conditions, suggesting that the effect of water on the t_{90} value was explainable by the plasticizing effect of absorbed water,

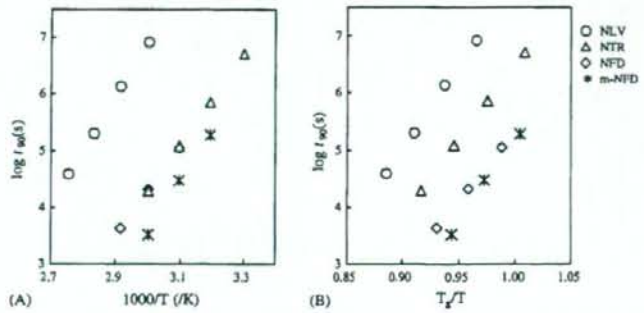

Fig. 4. Relationship between t_{90} for crystallization of drugs and storage temperature under dry conditions.

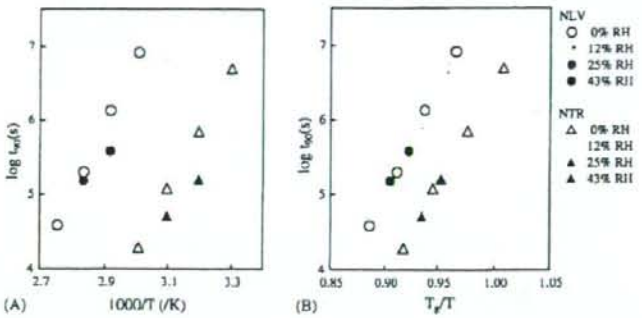

Fig. 5. Effect of absorbed water on the t_{90} of crystallization for NLV (circles) and NTR (triangles). The t_{90} values were measured at the early stage of crystallization at which no marked change in Tg was evident.

Table 2
T_g values of NTR-polymer solid dispersions

Polymer (%)	T_g (°C)	
	PVP	HPMC
0	32.4 ± 0.3	
3	33.2 ± 0.2	32.4 ± 0.1
5	34.1 ± 0.3	32.9 ± 0.4
6	34.1 ± 0.3	32.8 ± 0.2
11	36.6 ± 0.3	33.4 ± 0.3
20	–	33.7 ± 0.7
23	43.4 ± 0.8	–

similarly to that reported for NFD crystallization (Aso et al., 1995).

The effect of T_g on the crystallization rate of NTR was also investigated in solid dispersions with PVP and HPMC. A single T_g was observed for amorphous NTR-polymer solid dispersions prepared with 2.7–23% polymer excipients, indicating that NTR and polymer are miscible within the sensitivity limit of the DSC method. The value of T_g tended to increase with the amount of polymer, and the extent of increase was greater for NTR-PVP dispersions than for NTR-HPMC dispersions (Table 2). As the partially crystallized NTR-polymer dispersions showed a melt-

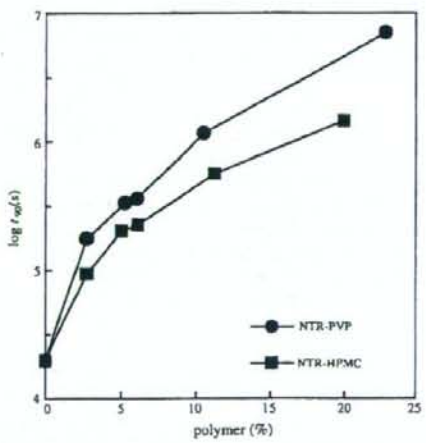

Fig. 6. Effect of polymer content on crystallization of NTR in solid dispersions with PVP and HPMC at 60 °C and 0%RH.

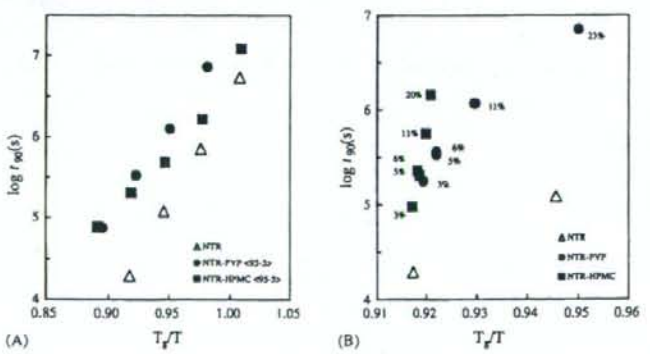

Fig. 7. Relationship between T_g/T and t_{90} of crystallization for NTR in the pure amorphous form and solid dispersions with PVP and HPMC. Numbers in percentage terms in figure (B) denote polymer contents.

ing peak at approximately 130 °C, the crystallization of NTR in the presence of the polymers was considered to be transition into a metastable form in a similar manner as that observed for pure amorphous NTR. Fig. 6 shows the effect of polymer excipients on the t_{90} values. Both PVP and HPMC increased t_{90} as the amount of polymer increased, but PVP was more effective in stabilizing amorphous NTR within the range of content studied. Fig. 7(A) shows the temperature dependence of t_{90} for solid dispersions containing 5% polymer. The t_{90} value compared at the same T_g/T was longer for both NTR-polymer dispersions than for pure NTR. Furthermore, the t_{90} versus T_g/T plots for solid dispersions containing various amounts of polymers did not overlap with that for pure NTR (Fig. 7(B)), indicating that crystallization of NTR was inhibited by the addition of PVP and HPMC to a greater extent than expected from the increased T_g. The present results imply that the drug-polymer interaction as well as an antiplasticizing effect of polymer excipients retarded the crystallization of the amorphous solid (Hirasawa et al., 2003a,b, 2004; Aso et al., 2004; Miyazaki et al., 2004, 2006; Wang et al., 2006).

Acknowledgement

A part of this work was supported by a grant from the Japan Health Science Foundation.

References

Andronis, V., Zografi, G., 2000. Crystal nucleation and growth of indomethacin polymorphs from the amorphous state. J. Non-Cryst. Solids 271, 236–248.

Aso, Y., Yoshioka, S., Otsuka, T., Kojima, S., 1995. The physical stability of amorphous nifedipine determined by isothermal microcalorimetry. Chem. Pharm. Bull. 43, 300–303.

Aso, Y., Yoshioka, S., Kojima, S., 2001. Explanation of the crystallization rate of amorphous nifedipine and Phenobarbital from their molecular mobility as measured by ^{13}C nuclear magnetic resonance relaxation time and the relaxation time obtained from the heating rate dependence of the glass transition temperature. J. Pharm. Sci. 90, 798–806.

Aso, Y., Yoshioka, S., Kojima, S., 2004. Molecular mobility-based estimation of the crystallization rates of amorphous nifedipine and Phenobarbital in poly(vinylpyrrolidone) solid dispersions. J. Pharm. Sci. 93, 384–391.

Burger, A., Koller, K.T., 1996. Polymorphism and pseudopolymorphism on nifedipine. Sci. Pharm. 64, 293–301.

Burger, A., Rollinger, J.M., Brüggeller, P., 1997. Binary system of (*R*)- and (*S*)-nitrendipine—polymorphism and structure. J. Pharm. Sci. 86, 674–679.

Hancock, B.C., Zografi, G., 1997. Characteristics and significance of the amorphous state in pharmaceutical systems. J. Pharm. Sci. 86, 1–12.

Hirasawa, N., Ishise, S., Miyata, H., Danjo, K., 2003a. Physicochemical characterization and drug release studies of Nilvadipine solid dispersions using water-insoluble polymer as a carrier. Drug Dev. Ind. Pharm. 29, 339–344.

Hirasawa, N., Ishise, S., Miyata, H., Danjo, K., 2003b. An attempt to stabilize Nilvadipine solid dispersion by the use of ternary systems. Drug Dev. Ind. Pharm. 29, 997–1004.

Hirasawa, N., Ishise, S., Miyata, H., Danjo, K., 2004. Application of Nilvadipine solid dispersion to tablet formulation and manufacturing using crospovidone and methylcellulose as dispersion carriers. Chem. Pharm. Bull. 52, 244–247.

Hirayama, F., Honjo, M., Arima, H., Okimoto, K., Uekama, K., 2000. X-ray crystallographic characterization of Nilvadipine monohydrate and its phase transition behavior. Eur. J. Pharm. Sci. 11, 81–88.

Kuhnert-Brandstätter, M., Völlenklee, R., 1986. Beitrag zur polymorphie von arzneistoffen 2. Mitteilung: halofenat, lorcainidhydrochlorid, minoxidil, mopidamol und nitrendipin. Sci. Pharm. 54, 71–82.

Miyazaki, T., Yoshioka, S., Aso, Y., Kojima, S., 2004. Ability of polyvinylpyrrolidone and polyacrylic acid to inhibit the crystallization of amorphous acetaminophen. J. Pharm. Sci. 93, 2710–2717.

Miyazaki, T., Yoshioka, S., Aso, Y., 2006. Physical stability of amorphous acetanilide derivatives improved by polymer excipients. Chem. Pharm. Bull. 54, 1207–1210.

Ngai, K.L., Magill, J.H., Plazek, D.J., 2000. Flow, diffusion and crystallization of supercooled liquids: revisited. J. Chem. Phys. 112, 1887–1892.

Rodríguez-Hornedo, N., Murphy, D., 1999. Significance of controlling crystallization mechanisms and kinetics in pharmaceutical systems. J. Pharm. Sci. 88, 651–660.

Saleki-Gerhardt, A., Zografi, G., 1994. Non-isothermal and isothermal crystallization of sucrose from the amorphous state. Pharm. Res. 11, 1166–1173.

Wang, L., Cui, F.D., Hayase, T., Sunada, H., 2005. Preparation and evaluation of solid dispersion for Nitrendipine-carbopol and Nitrendipine-HPMCP systems using a twin screw extruder. Chem. Pharm. Bull. 53, 1240–1245.

Wang, L., Cui, F.D., Sunada, H., 2006. Preparation and evaluation of solid dispersions of Nitrendipine prepared with fine silica particles using the melt-mixing method. Chem. Pharm. Bull. 54, 37–43.

Zhou, D., Zhang, G.G.Z., Law, D., Grant, K.J.W., Schmitt, E.A., 2002. Physical stability of amorphous pharmaceuticals: importance of configurational thermodynamic quantities and molecular mobility. J. Pharm. Sci. 91, 1863–1872.

ARTICLE IN PRESS
+ MODEL
Available online at www.sciencedirect.com
ScienceDirect
ELSEVIER
Biologicals xx (2007) 1–11
IABS BIOLOGICALS
www.elsevier.com/locate/biologicals

Influences of the recombinant artificial cell adhesive proteins on the behavior of human umbilical vein endothelial cells in serum-free culture

Akiko Ishii-Watabe [a,*], Toshie Kanayasu-Toyoda [b], Takuo Suzuki [a], Tetsu Kobayashi [a], Teruhide Yamaguchi [b], Toru Kawanishi [a]

[a] Division of Biological Chemistry and Biologicals, National Institute of Health Sciences, 1-18-1 Kamiyoga, Setagaya-ku, Tokyo 158-8501, Japan
[b] Division of Cellular and Gene Therapy Products, National Institute of Health Sciences, 1-18-1 Kamiyoga, Setagaya-ku, Tokyo 158-8501, Japan

Received 8 June 2006; revised 4 December 2006; accepted 22 December 2006

Abstract

To improve the safety of cellular therapy products, it is necessary to establish a serum-free cell culture method that can exclude animal-derived materials in order to avoid contamination with transmissible agents. It would be optimal if the proteins necessary to a serum-free culture could be provided as recombinant proteins. In this study, the influences of recombinant artificial cell adhesive proteins on the behavior of human umbilical vein endothelial cells (HUVECs) in serum-free culture were examined in comparison with the influence of plasma fibronectin (FN). The recombinant proteins used were Pronectin F (PF), Pronectin F PLUS (PFP), Pronectin L (PL), Retronectin (RN), and Attachin (AN). HUVECs adhered more efficiently on PF or PFP than on FN. No cells adhered on PL. Regarding the VEGF or bFGF-induced cell growth, the cells on PF and PFP proliferated at a similar rate to the cells on FN. RN and AN were less effective in supporting cell growth. Since cell adhesion on PF and PFP induced phosphorylation of focal adhesion kinase, they are thought to activate integrin-mediated intracellular signaling. The cells cultured on PF or PFP were able to produce prostaglandin I_2 or tissue-plasminogen activator in response to thrombin. However, thrombin caused detachment of the cells from PF but not from PFP or FN, meaning that the cells were able to adhere more tightly on PFP or FN than on PF. These data indicate that PFP could be applicable as a substitute for plasma FN.

Keywords: Cell adhesive protein; Recombinant protein; Fibronectin; Endothelial cells

1. Introduction

The widespread development of cellular therapy products has advanced to the stage of non-clinical and clinical testing [1–3]. Regulatory documents for human somatic cell therapy including instructions for investigational new drug applications have been published [4–6]. To guarantee the safety of both product recipients and the public at large, it is crucial to prevent contamination of cellular therapy products by infectious agents [7].

Serum-free culture is one of the desired methods for manufacturing cellular therapy products when safety issues are a concern [8,9]. Although serum is a very effective additive for a culture medium that can support cell adhesion, survival, growth, and functions, animal-derived materials such as serum may contain transmissible agents or human allergens [10–13]. Since serum is composed of proteins, sugars, lipids, vitamins, and other ingredients, its quality is affected by the genetic and environmental circumstances of the animal used, which means there are lot-to-lot variations in composition and potency. This variability could reduce the consistency of cellular therapy products, and a serum-free culture that could contribute to improving the consistency of the cell features is thus needed.

Protein factors often need to be added to serum-free culture to substitute for the functions of serum. The proteins used for this purpose must also pose no risk of infection. Because recombinant proteins can be produced without using animal-derived materials, and pose little risk of contaminating human pathogens, they are a useful biomaterial for culturing cells

* Corresponding author. Tel./fax: +81 3 3700 9084.
E-mail address: watabe@nihs.go.jp (A. Ishii-Watabe).

1045-1056/07/$32.00
doi:10.1016/j.biologicals.2006.12.002

when safety issues are a concern. In addition, the functions of recombinant proteins can be improved by modifying their amino acid sequences, which is also an advantage. In this study, using a serum-free culture of human umbilical vein endothelial cells (HUVECs), the usefulness of recombinant artificial cell adhesive proteins as a plasma fibronectin substitute was evaluated.

The extracellular matrix glycoprotein fibronectin consists of two similar polypeptide chains, each with a molecular mass of approximately 250 kDa joined at their respective C termini by disulfide bonds [14,15]. The RGD (arginine–glycine–aspartic acid) recognition sequence located within the molecule was the first amino acid motif shown to mediate cell adhesion [16,17]. Intracellular signaling induced by cell adhesion on fibronectin plays a critical role in cytoskeletal reorganization, cell cycle progression, and cell survival [18,19].

This study defines the influences of five different kinds of recombinant artificial cell adhesive proteins on endothelial adhesion, proliferation, and antithrombotic function in serum-free culture for which plasma fibronectin is needed. The recombinant proteins used were Pronectin F, Pronectin F PLUS, Pronectin L, Retronectin, and Attachin (Table 1).

2. Materials and methods

2.1. Recombinant cell adhesive proteins

Pronectin F, Pronectin F PLUS, and Pronectin L were purchased from Sanyo Chemical Industry (Kyoto, Japan), Retronectin from TaKaRa (Shiga, Japan), and Attachin from Bio999 (Taipei, Taiwan). All of these proteins were produced via bacterial fermentation. Pronectin F is a genetically engineered protein containing repeating units of the RGD sequence interspersed with a β-silk peptide for structural stability [20]. It is comprised of 980 amino acids. Based on its sequence, the molecular weight is estimated to be 72,728. The amino acid sequence is fMDPVVLQRRDWENPGVTQLNRLAA HPPFASDPMGAGS(GAGAGS)$_6$GAAVTGRGDSPASAAGY-[(GAGAGS)$_9$GAAVTGRGDSPASAAGY]$_{12}$-(GAGAGS)$_2$GA GAMDPGRYQLSAGRYHYQLVWCQK. Pronectin F PLUS is a positively charged water-soluble variant of Pronectin F that is produced by chemical modification [21,22]. Pronectin L is a protein polymer that exhibits IKVAV epitopes from the laminin alpha chain with a similar backbone as Pronectin F [21]. It is comprised of 1019 amino acids. The molecular weight is estimated to be 75,639. The amino acid sequence is fMDPVVLQRRDWENPGVTQLNRLAAHPPFASDPMGA GS(GAGAGS)$_6$GAAPGASIKVAVSAGPSAGY-[(GAGAGS)$_9$ GAAPGAIKVAVSAGPSAGY]$_{12}$-(GAGAGS)$_2$GAGAMDPG RYQLSAGRYHYQLVWCQK. Retronectin consists of a central cell-binding domain, a high affinity heparin-binding domain II, and a CS1 site within an alternatively spliced type III connecting segment region of human fibronectin [23]. It is comprised of 574 amino acids. The molecular weight is estimated to be 62,631. Attachin is an artificial fusion protein with the molecular weight of 30 kDa that has several functional domains, including a fibronectin-like cell attachment domain [24]. It has reportedly been used to promote the adhesion of several kinds of cell lines, including CHO-K1, MDBK, PK-15, L929, Vero, COS, U373, Swiss 3T3, and MRC-5 [25].

2.2. Cells and materials

Human umbilical vein endothelial cells (HUVECs) were purchased from Sanko Junyaku (Tokyo, Japan) and maintained

Table 1
Fibronectin and recombinant cell adhesive proteins used in this study

Proteins	Structure	Molecular Weight
Fibronectin	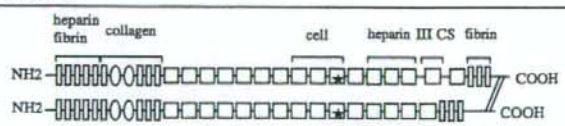	250K x 2
Pronectin F	Head-[(GAGAGS)9GAAVTGRGDSPASAAGY]12-Tail ★	73K
Pronectin F Plus	Positively charged, water-soluble variant of Pronectin F	73K
Pronectin L	Head-[(GAGAGS)9GAAPGASIKVAVSAGPSAGY]12-Tail ◆	76K
Retronectin	Chimeric protein of human fibronectin fragment 	63K
Attachin	A fusion protein constructed by molecular biotechnology	30K

Fibronectin.
▯ Type I module.
○ Type II module.
□ Type III module.
★: cell attachment sequence derived from fibronectin.
◆: cell attachment sequence derived from laminin.

Please cite this article in press as: Ishii-Watabe A et al., Influences of the recombinant artificial cell adhesive proteins on the behavior of human umbilical vein endothelial cells in serum-free culture, Biologicals (2007), doi:10.1016/j.biologicals.2006.12.002

in EGM-2 media (Cambrex, Walkersville, MD) on collagen-coated dishes (Asahi Techno Glass, Tokyo, Japan). EGM-2 media is modified MCDB 131 containing 2% fetal bovine serum, VEGF, bFGF, IGF-1, EGF, heparin, hydrocortisone and ascorbic acid. The cells were kept in a humidified, 5% CO_2 environment at 37 °C. Cells between passages 3 and 5 were used for all experiments.

The serum-free media used was human endothelial SFM (Invitrogen, Carlsbad, CA) [26]. Ten nanograms/ml of epidermal growth factor (EGF) (Invitrogen) and 20 ng/ml of basic fibroblast growth factor (bFGF) (Invitrogen) were added as supplements. Fibronectin is recommended for use as a cell attachment factor.

2.3. Cell adhesion assay

Recombinant cell adhesive proteins were diluted with phosphate buffered saline (PBS(−)), and plated on multiwell non-treated polystyrene plates (BD Falcon, Franklin Lakes, NJ). The plates were incubated for 2 h at room temperature, and then the protein solutions were removed and the wells washed with PBS(−). The concentration of the recombinant proteins used was 10 μg/ml (2 μg/cm^2), unless the description states otherwise. The amount of absorbed protein was quantified with a QuantiPro BCA Kit (Sigma, St. Louis, MO) using bovine serum albumin as a standard.

The HUVECs were harvested using trypsin and washed twice with PBS(−). The cells were then suspended in serum-free media, and added to each well of 96-well plates previously coated with recombinant cell adhesion proteins at a cell density of 1×10^4 cells/well. After incubating for 60 min under 5% CO_2 at 37 °C, the supernatant was removed, and the wells rinsed with PBS(−) to remove non-adherent cells. Following fixation of the adherent cells by 4% paraformaldehyde for 10 min, the paraformaldehyde was removed and the cells washed once with distilled water. A 0.5% (w/v) solution of crystal violet was then added to the wells. After staining for 25 min, the cells were rinsed five times with distilled water and the crystal violet that was absorbed on the adherent cells was solubilized with 0.5% SDS. The optical density at 595 nm was measured on an EL340 plate reader (BioTek Instruments, Winooski, VT).

2.4. Measurement of cell proliferation

HUVECs were harvested and suspended in serum free media, and plated to each well of the 96-well plates previously coated with recombinant cell adhesive proteins. VEGF (R&D Systems, Minneapolis, MN) or bFGF (Invitrogen, Carlsbad, CA) was added at concentrations of 1–100 ng/ml. After culturing for 2 days under 5% CO_2 at 37 °C, the cell number in each well was measured using Cell Counting Kit-8 (Dojindo, Kumamoto, Japan). Results are expressed as the mean value ± S.D. of triplicate determinations.

2.5. Phosphorylation of focal adhesion kinase

The HUVECs were collected by trypsin treatment (Invitrogen), resuspended in serum free medium, incubated for 2 h at 37 °C in suspension, and subsequently plated at 5×10^5 cells/dish on 60 mm diameter dishes pre-coated with cell adhesive proteins or bovine serum albumin (BSA) (10 μg/ml) [27]. After incubation for 2 h under 5% CO_2 at 37 °C, the cells were lysed in RIPA buffer (50 mM Tris–HCl (pH 7.6), 150 mM NaCl, 1% NP-40, 0.25% sodium deoxycholate), and the protein concentrations were determined using the BCA assay (Pierce, Rockford, IL). 3.5 μg of the total cell lysates was resolved by SDS–PAGE, blotted onto Immobilon-P membranes (Millipore, Volketswil, Switzerland), and incubated in 1% BSA with anti-pY397 FAK antibody (Upstate Biotechnology Inc.,, Lake Placid, NY) followed by incubation with horseradish peroxidase-labeled secondary antibody (Cell Signaling Technology, Danvers, MA). The ECL system (GE Healthcare Bio-Sciences AB, Uppsala, Sweden) and Luminoimage analyzer LAS 3000 (Fuji Film, Kanagawa, Japan) were used for detection. The membranes were stripped of bound antibody using a Re-Blot Plus Western Blot Recycling Kit (Chemicon, Temecula, CA), and the membrane was reprobed with anti-FAK antibody (Upstate Biotechnology). The labeled bands were quantified using the MultiGauge software program (Science Lab). The quantified value for phosphorylated FAK was normalized with that for total FAK in each sample, and the relative phosphorylation level was then calculated as a ratio against the cell lysate on fibronectin.

2.6. Secretion of Prostaglandin I_2 (PGI_2)

The HUVECs were harvested using trypsin, washed twice, and then suspended in serum-free media. The cells were placed on the 24-well plates coated with recombinant cell adhesive proteins at the density of 7×10^4/well. After culturing for 1 day, the cells were stimulated with 1 U/ml of thrombin or 30 ng/ml of VEGF. The cells were incubated for 1 h under 5% CO_2 at 37 °C, and then the supernatant was collected. The supernatant was centrifuged for 10 min at 2000 × g in a microcentrifuge to remove any residual cells. The level of 6-keto Prostaglandin $F_1\alpha$, a major metabolite of Prostaglandin I_2, was determined using 6-keto Prostaglandin $F_1\alpha$ EIA Kit (Cayman Chemical, Ann Arbor, MI). Each culture condition was repeated in triplicate.

2.7. Secretion of tissue-plasminogen activator

The HUVECs were seeded as described above. After culturing for 1 day, the cells were stimulated with 0.01–1 U/ml of thrombin. Twenty-four hours later, the supernatant was collected and spun down for 10 min at 2000 × g in a microcentrifuge. The level of tissue plasminogen activator was determined using the AssayMax Human Tissue-Type Plasminogen Activator ELISA Kit (Assay Pro, Brooklyn, NY). Each culture condition was repeated in triplicate. Phase contrast images were obtained before the supernatant was collected.

Please cite this article in press as: Ishii-Watabe A et al., Influences of the recombinant artificial cell adhesive proteins on the behavior of human umbilical vein endothelial cells in serum-free culture, Biologicals (2007), doi:10.1016/j.biologicals.2006.12.002

3. Results

3.1. Adhesion of HUVECs onto recombinant cell adhesive proteins

To examine the adhesion onto the recombinant cell adhesive proteins, HUVECs harvested and suspended in serum-free media were applied on plastic wells precoated with Pronectin F, Pronectin F PLUS, Pronectin L, Retronectin, Attachin, or fibronectin (Table 1). As shown in Fig. 1, Pronectin F, Pronectin F PLUS, Retronectin, or Attachin showed cell adhesion activity to a similar extent as fibronectin at the concentration of 10 μg/ml (2 μg/cm^2). Pronectin F and Pronectin F PLUS were superior to fibronectin when they were used at an amount of less than 1 μg/ml. The cells were observed under microscopy to have spread well on the recombinant proteins that they adhered to (Fig. 2). No cells had adhered onto Pronectin L or BSA.

In order to test if these differences are due to the difference in the absorbed amount of each protein, the protein absorbed on the plate was measured (Fig. 3). It was found that Pronectin F and Pronectin L had absorbed to the plate better than other proteins and that the absorbed amount of Pronectin F PLUS was lower than that of Pronectin F and Pronectin L. From the point of view of the efficiency of cell adhesion (Fig. 1) and the absorbed amount of protein (Fig. 3), the number of cells attached was not dependent on the amount of absorbed protein, suggesting that the observed effects were not due to differences in protein absorption but rather due to the character of each cell adhesion protein.

3.2. Influences on cell proliferation

Besides anchorage, cell adhesion to components of the extracellular matrix triggers signaling events affecting diverse cellular traits and activities, including survival, proliferation, and other functions. Therefore, the influences of the recombinant cell adhesion proteins on cell proliferation were examined. The HUVECs in serum-free media were seeded on the plates that were coated with recombinant cell adhesive proteins, and then cultured in the presence or absence of basic fibroblast growth factor (bFGF) or vascular endothelial growth factor (VEGF) at concentrations from 1 to 100 ng/ml. After culturing for 2 days, the cell numbers in each well were examined (Fig. 4). When HUVECs were cultured in the presence of bFGF, the cells on Pronectin F or Pronectin F PLUS had grown to the same level as that on fibronectin in each concentration of bFGF, showing that Pronectin F and Pronectin F PLUS have the same growth support potency as fibronectin (Fig. 4A). However, the cell numbers on Retronectin or Attachin reached 70% or 40% of that on fibronectin, respectively; showing that the growth support potency of Retronectin and Attachin was lower than fibronectin. When VEGF-stimulated cell proliferation was examined, Pronectin F and Pronectin F PLUS also showed similar growth-supporting potency to fibronectin (Fig. 4B). Retronectin and Attachin were less effective than fibronectin.

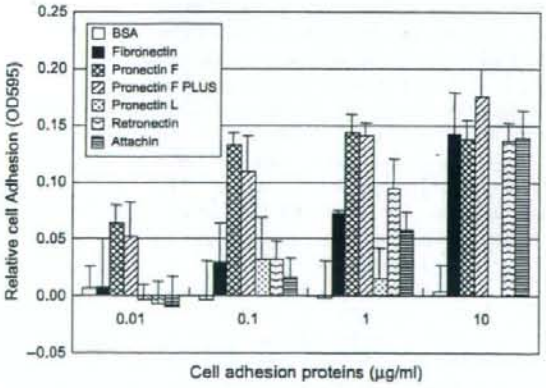

Fig. 1. Adhesion of HUVECs to recombinant cell adhesive proteins. HUVECs were plated into wells previously coated with Fibronectin, Pronectin F, Pronectin F PLUS, Pronectin L, Retronectin, Attachin, or BSA, and then incubated for 1 h at 37 °C. Attached cells were fixed and stained with crystal violet and quantified by absorbance reading. Results are expressed as mean value ± S.D. of triplicate determinations. The 0.1 OD corresponded to $0.61 \pm 0.085 \times 10^4$ cells.

3.3. Phosphorylation of focal adhesion kinase

Cell adhesive proteins activate intracellular signaling via cell surface integrins. In regulating the cellular responses to integrin-mediated adhesion, focal adhesion kinase (FAK) has emerged as a key signaling molecule [28–30]. Integrin–ligand engagement promotes FAK tyrosine phosphorylation that promotes FAK signaling activity. The phosphorylation of FAK Tyr-397, the only apparent autophosphorylation site, is known to create a high-affinity binding site for SH2 domains of the Src-family kinases, including c-Src and Fyn [31].

HUVECs cultured in growing media were harvested by trypsin treatment, and incubated in serum-free media for 2 h at 37 °C in suspension. After this incubation, the cells were plated onto the dishes in which recombinant cell adhesive proteins were coated, and then incubated for 2 h under 5% CO_2 at 37 °C. Cell lysates were prepared using RIPA buffer, and the phosphorylation level of FAK on Tyr 397 was then examined by Western blotting. As shown in Fig. 5, FAK Tyr-397 is phosphorylated under an attached condition (lane 1), becomes dephosphorylated upon cell suspension (lane 2), and then becomes rephosphorylated after replating. The FAK phosphorylation level after replating on recombinant proteins differed in each sample (lanes 3–10). Phosphorylation level of cells on BSA (lane 3) or Pronectin L (lane 7), to which cells did not adhere, was still lower after replating. Pronectin F (lane 5) or Pronectin F PLUS (lane 6) induced FAK phosphorylation to the similar extent to Fibronectin (lane 4), suggesting that Pronectin F and Pronectin F PLUS are thought to activate intracellular signaling via integrin as well as fibronectin. Retronectin that has RGD domain of Fibronectin also induced FAK phosphorylation (lane 8).

Please cite this article in press as: Ishii-Watabe A et al., Influences of the recombinant artificial cell adhesive proteins on the behavior of human umbilical vein endothelial cells in serum-free culture, Biologicals (2007), doi:10.1016/j.biologicals.2006.12.002

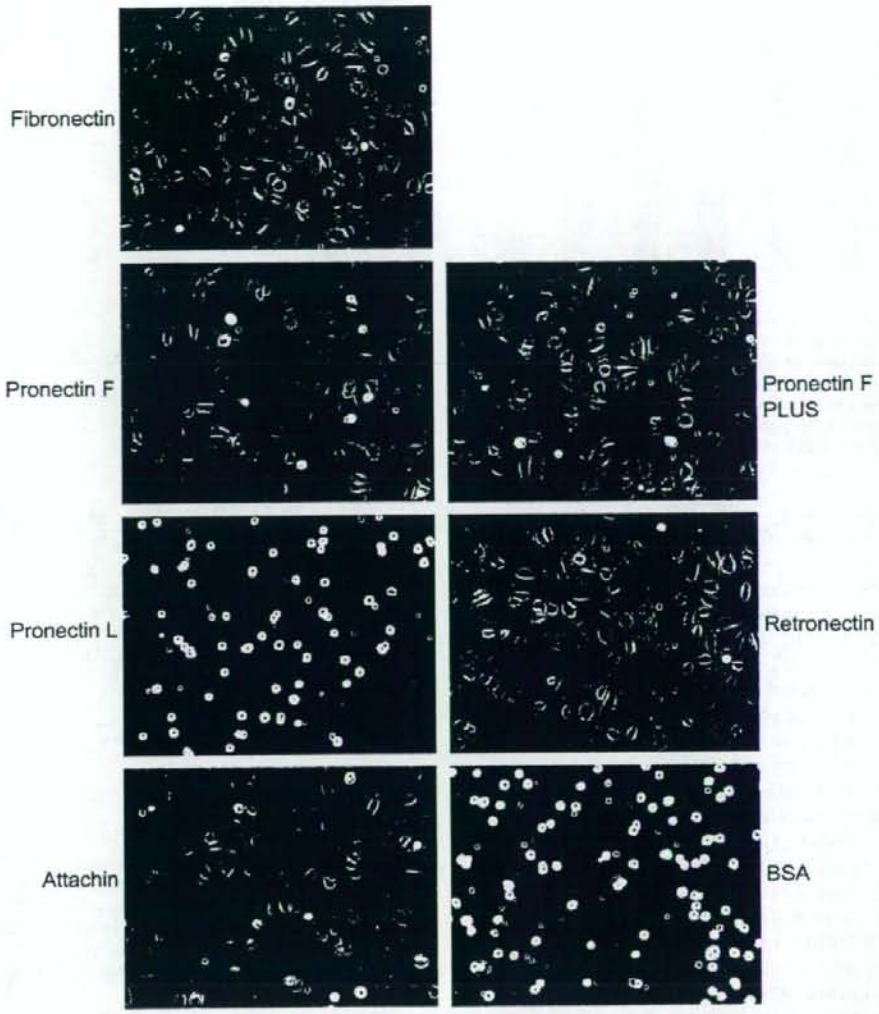

Fig. 2. The phase contrast images of cell attachment and spreading on recombinant cell adhesive proteins. HUVECs were seeded into wells previously coated with 10 μg/ml of Fibronectin, Pronectin F, Pronectin F PLUS, Pronectin L, Retronectin, Attachin, or BSA. After 1 h incubation at 37 °C, the cells were photographed with an inverted microscope.

3.4. Influences on antithrombotic functions of endothelial cells

In order to examine the influences of recombinant cell adhesive proteins on cellular functions, the production of prostaglandin I_2 (PGI_2) and tissue-plasminogen activator (t-PA), both of which play important roles in the antithrombotic feature of endothelial cells, was tested. Antithrombotic activity is the most important characteristic of endothelial cells that are used for artificial blood vessels or engineered vascularized tissues. PGI_2 inhibits platelet aggregation, thereby inhibiting the formation of thrombus. It is produced quickly after stimulation via the activation of phospholipase A_2. Since the half life of PGI_2 is as short as 2 min, the concentrations of its metabolite 6-keto Prostaglandin $F_1\alpha$ were measured. t-PA is produced from endothelial cells via the induction of protein synthesis in response to the extracellular stimuli. It induces the processing of plasminogen to plasmin, and dissolves the fibrin clots.

HUVECs were plated on the recombinant cell adhesion protein-coated dishes and cultured for 1 day, then stimulated with VEGF or thrombin. As shown in Fig. 6A, PGI_2 was produced from VEGF- stimulated HUVECs on different kinds of cell adhesive proteins to the same level. In the serum-free media, the basal production of PGI_2 was higher, and the production after the stimulation was less than in the growing

Please cite this article in press as: Ishii-Watabe A et al., Influences of the recombinant artificial cell adhesive proteins on the behavior of human umbilical vein endothelial cells in serum-free culture, Biologicals (2007), doi:10.1016/j.biologicals.2006.12.002

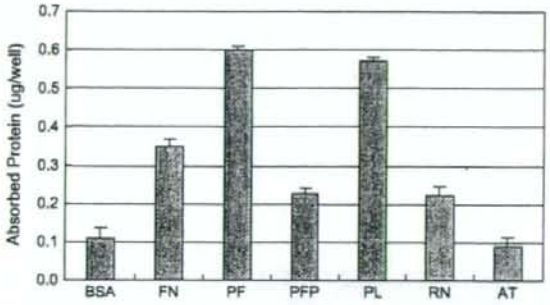

Fig. 3. Protein absorption on non-treated polystyrene plates. Ten μg/ml of bovine serum albumin (BSA), Fibronectin (FN), Pronectin F (PF), Pronectin F PLUS (PFP), Pronectin L (PL), Retronectin (RN) or Attachin (AN) was added to 96-well plates and incubated at room temperature for 2 h. Each well was washed with PBS(−) and the amount of absorbed protein was quantitated by QuantiPro BCA using bovine serum albumin as a standard. Each data point represents the mean ± S.D. of triplicate determinations.

media. Similar results were obtained when the cells were stimulated with thrombin (Fig. 6B).

Next, t-PA production from the thrombin-stimulated HUVECs was examined. As shown in Fig. 7, the t-PA concentration in the culture supernatant of HUVECs that adhered on Pronectin F PLUS was the same as that on Fibronectin. However, the concentration was lower in the supernatant on Pronectin F, Retronectin, or Attachin than on fibronectin. The basal production of t-PA in the serum-free media was less than in growing media; therefore, responsiveness to thrombin was readily observed in the serum-free culture.

During these experiments using thrombin, detachment of the thrombin-stimulated cells from Pronectin F, Retronectin, or Attachin was observed (Fig. 8). No detachment was seen in the cells that adhered on fibronectin or Pronectin F PLUS. This result might reflect the possibility that the adhesiveness of the cells to Pronectin F, Retronectin, and Attachin is weaker than to Pronectin F PLUS or fibronectin.

The following data support the results of Fig. 8, which are presented using microscopic images. Since HUVECs are adherent cells, detachment from the dishes leads to a loss of viability. Therefore, changes in the viable cell concentration after thrombin stimulation reflect cell detachment. As shown in Fig. 9, the production of t-PA and changes in the viable cell concentration after culturing in the presence of 0.01, 0.1, or 1 U/ml of thrombin were tested. At all three concentrations of thrombin used, cell detachment was observed only from Pronectin F. Although the t-PA concentration was increased in a dose-dependent manner by thrombin in the cells that adhered on Fibronectin or Pronectin F PLUS (Fig. 9A), there was less of an increase in t-PA production from the cells on Pronectin F when a low dose (0.01 or 0.1 U/ml) of thrombin was used. At those concentrations, the viable cell concentration on Pronectin F was decreased by thrombin stimulation, meaning that cell detachment occurred on Pronectin F (Fig. 9B). At a high concentration of thrombin (1 U/ml), the viable cell concentration decreased slightly even though cell detachment was

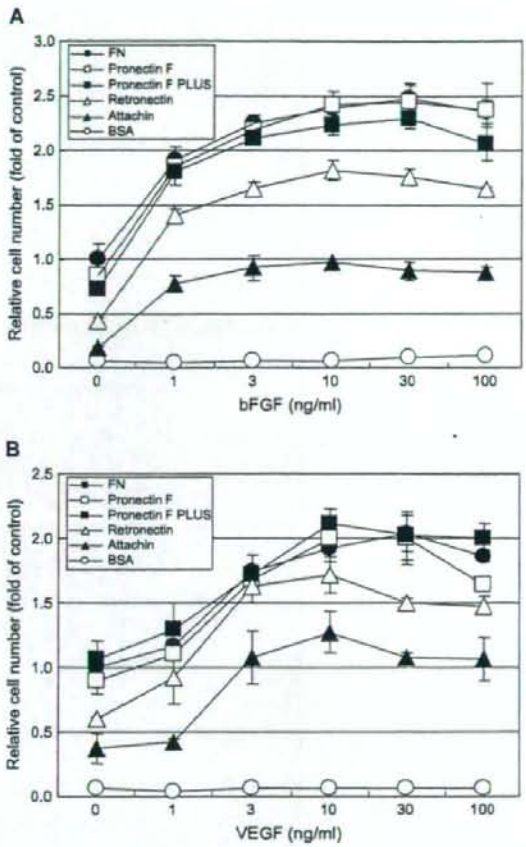

Fig. 4. Effects of recombinant cell adhesive proteins on the VEGF- or bFGF-induced cell proliferation. HUVECs were seeded into wells previously coated with 10 μg/ml of Fibronectin, Pronectin F, Pronectin F PLUS, Retronectin, Attachin, or BSA, and cultured for 2 days in the presence or absence of bFGF (A) or VEGF (B) at the concentrations indicated. The relative cell number was examined using a cell counting kit-8. The results are expressed as the mean value ± S.D. of triplicate determinations.

observed. This might be because the cell proliferative effect of thrombin canceled the decrease in cell viability. t-PA production corrected by the viable cell concentration is shown in Fig. 9C. By correcting the t-PA concentration using the viable cell concentration, the dose-dependency of thrombin in t-PA production was similar in Pronectin F to Pronectin F PLUS and fibronectin (Fig. 9C). From these results, in the cells on Pronectin F and Pronectin F PLUS, the signals from thrombin transduced similarly, but the strength of the cell adhesion differed.

4. Discussion

The goal of the present study was to establish a cell culture method that can improve the safety of cellular therapy products. Our focus is now on human endothelial cells, because

Please cite this article in press as: Ishii-Watabe A et al., Influences of the recombinant artificial cell adhesive proteins on the behavior of human umbilical vein endothelial cells in serum-free culture, Biologicals (2007), doi:10.1016/j.biologicals.2006.12.002